TRANSIENT MULTIPHASE FLOW PHENOMENA AND DEFECT FORMATION IN STEEL CONTINUOUS CASTING

Allocation: Illinois/100 Knh
PI: Brian G. Thomas[1,2]
Co-PIs: Seong-Mook Cho[1], Surya Pratap Vanka[1], Hyunjin Yang[1], Matthew Zappulla[2], Ahmed Taha3, Seid Koric[1,3]

[1]University of Illinois at Urbana-Champaign
[2]Colorado School of Mines
[3]National Center for Supercomputing Applications

MP

EXECUTIVE SUMMARY

The objective of this project is to develop computational models to simulate transient multiphase flows and related phenomena, to apply them to gain an improved fundamental understanding of defect formation in continuous steel casting, and to find ways to further improve the process. Large-Eddy Simulations (LES) coupled with a Volume of Fluid (VOF) model were applied to track transient motion of the liquid mold flux/molten steel interface and slag entrainment into the molten steel pool during steady state continuous casting. In addition, the transport of argon bubbles in the molten steel and their capture into the solidifying steel shell were simulated using LES simulations coupled with a Lagrangian Discrete Phase Model for particle transport and particle capture criteria. Furthermore, the LES models were validated with facility measurements and applied to investigate optimal process conditions for the nozzle port angle, submergence depth of the nozzle, and Electro-Magnetic Braking (EMBr) field strength. These simulations on Blue Waters reveal deeper insights into defect formation during the continuous casting of steel and have enabled improved operation.

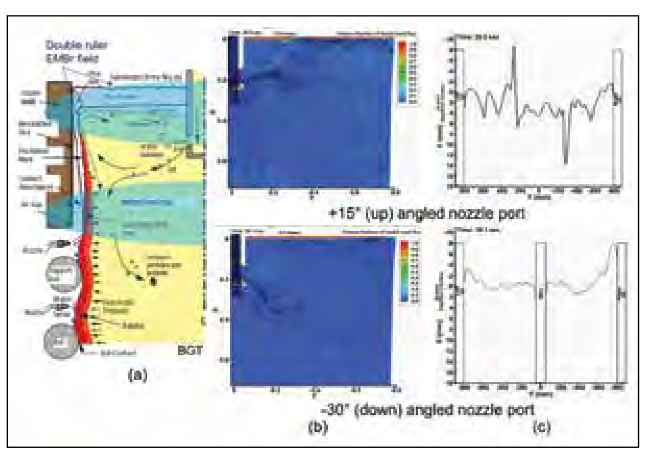

Figure 1: (a) Schematic of multiphase flow phenomena in the steel continuous-casting mold and Effect of nozzle port angle on (b) mold flow patterns, including motion of the top liquid mold flux layer, and (c) level variations at the liquid mold flux/molten steel interface in the meniscus region.

RESEARCH CHALLENGE

Continuous casting is the most widely employed solidification-process for steel manufacturing in the world [1], so even small improvements in this important process can lead to large benefits. Most defects in final products are related to transient multiphase flow phenomena in the mold region of the process (Fig. 1(a)). Severe instability at the liquid mold flux/molten steel interface can entrain some of the liquid mold flux (added on top of the molten steel pool in the mold to prevent steel oxidation) into the molten steel [2]. In addition, argon gas bubbles, injected to prevent nozzle clogging [3], can be trapped by the solidifying steel shell in the mold. To reduce these problems, transient multiphase flow phenomena should be understood, and process conditions should be optimized to reduce defect formation during continuous casting.

In this year's project, LES of several different important aspects of multiphase flow were performed to quantify the transient liquid mold flux/molten steel interface, transport of argon gas bubbles, and bubble capture into the steel shell in the mold during nominally steady continuous casting of steel slabs for different process conditions. The modeling results have been validated with plant measurements and applied to find optimal process conditions, including nozzle port angle, nozzle submergence depth, and EMBr field strength.

METHODS & CODES

LES coupled with VOF were applied to model transient molten steel flow and to track the liquid mold flux/molten steel interface. These models were implemented into the commercial package ANSYS Fluent on Blue Waters (BW) XE nodes. To calculate bubble transport and capture into solidifying steel shells with and without EMBr, LES coupled with Lagrangian particle capture (based on a force balance on each particle at the solidification front) [5] and MagnetoHydroDynamics models [8] using the GPU-based in-house code CUFLOW were employed on BW XK nodes.

RESULTS & IMPACT

Turbulent swirl flow from the upward-angled nozzle ports produces jet wobbling in the mold [4]. Sometimes, the jet impinges onto the liquid mold flux/molten steel interface and drags some of the liquid mold flux into the steel pool, resulting in slag entrainment, as shown in Fig. 1(b). Most of the entrained slag becomes entrapped into the solidifying steel shell to form defects. Calculated interface instability reveals level variations greater than ~20 mm, especially at the meniscus region around its perimeter (Fig. 1(c)). These severe level instabilities can cause the liquid mold flux to touch the solidifying steel shell, and to be captured into the steel shell via meniscus hooks. However, the jet flow from the downward-angled nozzle ports with well-optimized casting conditions makes a classic double-roll pattern with less jet wobbling, resulting in better stability of the surface level and velocity in the mold. Velocity variations are smaller and the interface shows only ~2 mm fluctuations, so slag entrapment defects are drastically reduced.

Argon bubble motion is affected by turbulent jet flow in the mold, as shown in Fig. 2(a). Most bubbles larger than 3-mm in diameter float up toward the top surface due to their large buoyancy. On the other hand, small bubbles move along with the jet flow and easily reach the narrow face to be carried deep into the mold cavity. Many of the small bubbles move between the dendrites to be captured into the steel, especially without EMBr. However, EMBr slows and deflects the jet flow [6–7], so more bubbles float upward near the nozzle and fewer bubbles are transported to the narrow face and deep into the mold. As shown in Fig. 2(b), the bubble capture rate increases with time (until ~15-18 sec after gas injection for EMBr off and ~15 sec for EMBr on, because the jet flow path is shorter with EMBr). Then, after the flow has stabilized at nominally steady casting, EMBr is observed to reduce bubble entrapment significantly.

Parametric studies with these multiphase LES models have enabled better understanding of the complex multiphysics phenomena related to defect formation, including slag entrainment, inclusion and bubble transport, and capture. This has led to suggestions of nozzle geometry/casting condition combinations that lead to fewer defects, and, consequently, to significant savings to the steel plants.

WHY BLUE WATERS

Blue Waters enabled high-resolution multiphase flow simulations of the continuous caster needed for accurate predictions. In particular, the transient transport of small volume secondary-phases (entrained liquid mold slag and argon bubbles) in the turbulent flow require very small cells (~1 mm^3) in a huge domain, and simulations of over 50-seconds flow time (with 0.001-second time steps). Furthermore, Blue Waters resources (both ANSYS Fluent HPC on XE nodes and our in-house multi-GPU code CUFLOW on XK nodes) showed speed-up breakthroughs (e.g., over 3000x with ANSYS Fluent HPC on BW) needed to provide this modeling capability for the steel continuous casting process.

PUBLICATIONS AND DATA SETS

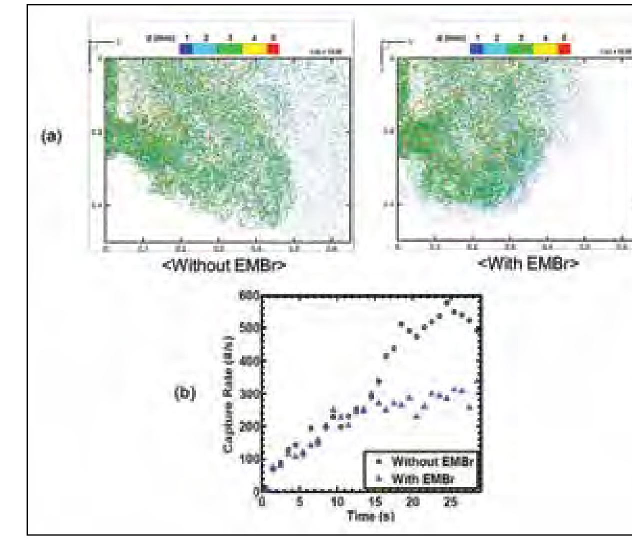

Figure 2: Effect of EMBr on (a) instantaneous argon bubble distributions and (b) bubble capture rate in the mold.

Cho, S.-M., et al., Effect of Nozzle Port Angle on Transient Mold Flow, Surface Level, and Heat Transfer in Steel Caster. *CCC Annual Report*, Golden, Colo., August 16–18, 2016.

Jin. K., P. Kumar , S. P. Vanka, and B.G. Thomas, Rise of an argon bubble in liquid steel in the presence of a transverse magnetic field. *Physics of Fluids*, 28:9 (2016), DOI: 10.1063/1.4961561.

Jin, K., S. P. Vanka, R. K. Agarwal, and B. G. Thomas, GPU Accelerated Simulations of Three-Dimensional Flow of Power-law Fluids in a Driven Cube. I*nt. J. Computational Fluid Mechanics,* 31:1 (2017), pp. 1029–0257. DOI 10.1080/10618562.2016.1270449.

Jin, K., S. P. Vanka, and B. G. Thomas, Large Eddy Simulation of the Effects of EMBr and SEN Submerged Depth on Turbulent Flow in the Mold Region of a Steel Caster. *Metallurgical and Materials Transactions B*, 48:1 (2016), pp. 162–178, DOI: 10.1007/s11663-016-0801-z.

Jin, K., S. P. Vanka, and B.G. Thomas, Large Eddy Simulations of Argon Bubble Transport and Capture in Mold Region of a Continuous Steel Caster. *Proc. TFEC2017*, Las Vegas, Nev., April 2–5, 2017.

Mackenzie, Paul

[1] Komijani, J., et. al, Decay constants fB and fBs and quark masses mb and mc from HISQ simulations. in *Proceedings of the 34th International Symposium on Lattice Field Theory* (Lattice, Southampton, UK, July 24–30, 2016).

Militzer, Burkhard

[1] Betti, R., editor. *Advancing the Science of High Energy Density Laboratory Plasmas* (2009).
[2] Cook, I., Materials research for fusion energy. *Nat. Mater.*, 5 (2006), DOI: 10.1038/nmat1584.
[3] Cauble, R., et al., Experiments Using Laser driven Shock-waves for EOS and Transport Measurements. *Contrib. Plasma Physics*, 41:2 (2001), pp. 239–242.
[4] Van Horn, H. M., Dense astrophysical plasmas. *Science*, 252 (1991), pp. 384–389.
[5] Militzer, B., Path Integral Monte Carlo Simulations of Hot Dense Hydrogen. Ph.D. thesis, University of Illinois at Urbana-Champaign (2000).
[6] Ceperley, D.M., Path integral in the theory of condense helium. *Rev. Mod. Phys.*, 67:2 (1995), DOI: 10.1103/RevModPhys.67.279.
[7] Militzer, B., F. Soubiran, S. M. Wahl, and W. Hubbard, Understanding Jupiter's Interior. *J. Geophysical Research*, 121:9 (2016), DOI: 10.1002/2016JE005080.
[8] Kresse, G., and J. Furthmuller, Efficient iterative schemes for *ab initio* total-energy calculations using a plane-wave basis set. *Phys. Rev. B*, 54:16 (1996), DOI: 10.1103/PhysRevB.54.11169.
[9] Zhang, S., K. P. Driver, F. Soubiran, and B. Militzer, First-principles equation of state and shock compression predictions of warm dense hydrocarbons. *Phys. Rev. E*, 96:1 (2017), DOI:10.1103/PhysRevE.96.013204.

Rani, Sarma

[1] Rani, S.L., R. Dhariwal, and D.L. Koch, A stochastic model for the relative motion of high Stokes number particles in isotropic turbulence. *Journal of Fluid Mechanics*, 756 (2014), pp. 870–902.
[2] D. Pekurovsky, P3DFFT: A framework for parallel computations of Fourier transforms in three dimensions. *SIAM J. Sci. Comput.*, 34:4 (2012), pp. C192–C209.
[3] Février, P., O. Simonin, and D. Legendre, Particle dispersion and preferential concentration dependence on turbulent Reynolds number from direct and large-eddy simulations of isotropic homogeneous turbulence. *Proceedings of the Fourth International Conference on Multiphase Flow* (New Orleans, La., May 27–June 1, 2001).
[4] Zaichik, L. I., O. Simonin, and V.M. Alipchenkov, Two statistical models for predicting collision rates of inertial particles in homogeneous isotropic turbulence. *Physics of Fluids*, 15:10 (2003), pp. 2995–3005.
[5] Dhariwal, R., S.L. Rani, and D.L. Koch, Stochastic Theory and Direct Numerical Simulations of the Relative Motion of High-Inertia Particle Pairs in Isotropic Turbulence. *Journal of Fluid Mechanics*, 813 (2017), pp. 205–249.

Riedl, Caroline

[1] The DOE/NSF Nuclear Science Advisory Committee Working Group, *The Frontiers of Nuclear Science: A Long-Range Plan* (2007), arXiv:0809.3137.
[2] Deshpande, A., et al., Electron Ion Collider: The Next QCD Frontier—Understanding the glue that binds us all. *European Physical Journal*, A:52 (2016), p. 268.
[3] Riahi H., et al., FTS3: Quantitative Monitoring. *Journal of Physics: Conference Series 664* (2015), DOI: 10.1088/1742-6596/664/6/062051.
[4] Allison J., et al., Facilities and Methods: Geant4—A Simulation Toolkit. *Nuclear Instruments and Methods in Physics Research*, A:506 (2003), pp. 250–303.
[5] Meyer, M., Blue Waters, A Petascale Computer Facility for the Reconstruction of CERN COMPASS-II data. *22nd International SPIN Symposium*, Urbana, Ill., September 26–30, 2016.
[6] Sjoestranda, T., et al., An Introduction to PYTHIA 8.2. *Computer Physics Communications*, 191 (2015), pp. 159–177.

Schleife, Andre

[1] Gajdos, M., et al., Linear optical properties in the projector-augmented wave methodology. *Phys. Rev. B*, 73:4 (2006), DOI: 10.1103/PhysRevB.73.045112.
[2] Kresse, G., and D. Joubert, From ultrasoft pseudopotentials to the projector augmented-wave method. *Phys. Rev. B*, 59:3 (1999), DOI: 10.1103/PhysRevB.59.1758.
[3] Kresse, G., and J.Furthmüller, Efficient iterative schemes for *ab initio* total-energy calculations using a plane-wave basis set. *Phys. Rev. B*, 54:16 (1996), DOI: 10.1103/PhysRevB.54.11169.
[4] Rödl, C., F. Fuchs, J. Furthmüller, and F. Bechstedt, *Ab initio* theory of exitons and optical properties for spin-polarized systems: Application to antiferromagnetic MnO. *Phys. Rev. B*, 77:18 (2008), DOI: 10.1103/PhysRevB.77.184408.
[5] Fuchs, F., C. Rödl, A. Schleife, and F. Bechstedt, Efficient $O(N^2)$ approach to solve the Bethe–Salpeter equation for excitonic bound states. *Phys. Rev. B*, 78:8 (2008), DOI: 10.1103/PhysRevB.78.085103.
[6] Jun Lim, S., A. Schleife, and A. M. Smith, Optical determination of crystal phase in semiconductor nanocrystals. *Nat. Comm.*, 8 (2017), DOI: 10.1038/ncomms14849.

Taha, Ahmed

[1] Idkaidek, A., V. Agarwal, and I. Jasiuk, Finite element simulation of Reference Point Indentation on bone. *Journal of the Mechanical Behavior of Biomedical Materials*, 65 (2017), pp. 574–583.
[2] Idkaidek, A., and I. Jasiuk, Cortical bone fracture analysis using XFEM—case study. *International Journal for Numerical Methods in Biomedical Engineering*, 33: e2809 (2016), DOI: 0.1002/cnm.2809.

Thomas, Brian

[1] *Steel Statistical Yearbook 2014* (World Steel Association, Brussels, Belgium, 2014).
[2] Cho, S.-M., et al., Effect of Nozzle Clogging on Surface Flow and Vortex Formation in the Continuous Casting Mold. *Iron and Steel Technology*, 9 (2012), pp. 85–95.
[3] Rackers, K., and B. G. Thomas, Clogging in Continuous Casting Nozzles. *Proc. of 78th Steelmaking Conference* (Iron and Steel Society, Warrendale, Pa., 1995), pp. 723–734.
[4] Cho, S.-M., B. G. Thomas, H.-J. Lee, and S.-H. Kim, Effect of Nozzle Port Angle on Mold Surface Flow in Steel Slab Casting. *Iron and Steel Technology*, 3 (2017), pp. 76–84, reprinted from *Proceedings of AISTECH2016*.
[5] Jin, K., B. G. Thomas, and X. Ruan, Modeling and Measurements of Multiphase Flow and Bubble Entrapment in Steel Continuous Casting. *Metallurgical and Materials Transactions B*, 47:1 (2016), pp. 548–565, DOI: 10.1007/s11663-015-0525-5.
[6] Cho, S.-M., B. G. Thomas, and S.-H. Kim, Transient Two-Phase Flow in Slide-Gate Nozzle and Mold of Continuous Steel Slab Casting with and without Double-Ruler Electro-Magnetic Braking. *Metallurgical and Materials Transactions B*, 47:5 (2016), pp. 3080–3098, DOI: 10.1007/s11663-016-0752-4
[7] Jin, K, S. P. Vanka, B. G. Thomas, and X. Ruan, Large Eddy Simulations of the Effects of Double-Ruler Electromagnetic Braking and Nozzle Submergence Depth on Molten Steel Flow in a Commercial Continuous Casting Mold. *Proc. TMS Annual Meeting 2016* (The Minerals, Metals and Materials Society, Nashville, Tenn., February 14–18, 2016), pp. 159–166.
[8] Jin, K., P. Kumar, S. P. Vanka, and B.G. Thomas, Rise of an argon bubble in liquid steel in the presence of a transverse magnetic field. *Physics of Fluids*, 28:9 (2016), DOI: 10.1063/1.4961561.

Tinoco Lopez, Rafael

[1] Koch, E. W., Beyond light: physical, geological, and geochemical parameters as possible submersed aquatic vegetation habitat requirements. *Estuaries*, 24:1 (2001), pp. 1–17.
[2] Nepf, H. M., Hydrodynamics of vegetated channels. *Journal of Hydraulic Research*, 50:3 (2012), pp. 262–79.
[3] Nepf, H. M., Flow and transport in regions with aquatic vegetation. *Ann. Rev. Fluid Mech.*, 44 (2012), pp. 123–142.
[4] Tinoco, R., G. Coco, A laboratory study on sediment resuspension within arrays of rigid cylinders. *Adv. Water Res.*, 92 (2016), pp. 1–9.
[5] Dutta, S., et al., Application of computational fluid dynamic modelling to improve flow and grit transport in Terence J. O'Brien water reclamation plant, Chicago, Illinois. *J. Hydrl. Res.*, 52:6 (2014), pp. 759–774.
[6] Fischer, P. F., J. W. Lottes, and S. G. Kerkemeier, *Nek5000* webpage (2008), http://nek5000.mcs.anl.gov.
[7] Deville, M., P. Fischer, and E. Mund, *High-Order Methods for Incompressible Fluid Flow*. (Cambridge University Press, Cambridge, England, 2002.)

Wagner, Lucas

[1] Wagner, L.K., M. Bajdich, and L. Mitas, QWalk: A quantum Monte Carlo program for electronic structure. *Journal of Computational Physics*, 228 (2009), pp. 3390–3404.
[2] Zheng, H., and L.K. Wagner, Computation of the correlated metal-insulator transition in vanadium dioxide from first principles. *Physical Review Letters*, 114 (2015), 176401.
[3] Cao, J., et al., Strain engineering and one-dimensional organization of metal–insulator domains in single-crystal vanadium dioxide beams. *Nat Nano*, 4 (2009), pp. 732–737.

Yeung, Pui-kuen

[1] Frisch, U. *Turbulence: The Legacy of A.N. Kolmogorov*. Cambridge University Press (1995).
[2] Yeung, P. K., X. M. Zhai, and K. R. Sreenivasan, Extreme events in computational turbulence. *Proceedings of the National Academy of Sciences of the U.S.A.*, 112:41 (2015), pp. 12633–12638.
[3] Gotoh, T., S. Hatanaka, and H. Miura, Spectral compact difference hybrid computation of passive scalar in isotropic turbulence. *Journal of Computational Physics*, 231:21 (2012), pp. 7398–7414.
[4] Clay, M. P., D. Buaria, T. Gotoh, and P. K. Yeung, A dual communicator dual grid-resolution algorithm for petascale simulations of turbulent mixing at high Schmidt number. *Computer Physics Communications*, in press (2017), DOI: 10.1016/j.cpc.2017.06.009).

COMPUTER SCIENCE & ENGINEERING

Cox, Donna

[1] O'Shea, B., et al., Probing the Ultraviolet Luminosity Function of the Earliest Galaxies with the Renaissance Simulations. *The Astrophysical Journal Letters*, 807:1 (2015), DOI:10.1088/2041-8205/807/1/L12.
[2] Chen, P., Norman, L., Xu, H., and Wise, J. Fully Coupled Simulation of Cosmic Reionization. III. Stochastic Early Reionization by the Smallest Galaxies. Submitted to *The Astrophysical Journal*. Preprint at arXiv:1705.00026v1 [astro-ph.CO].